Mon. Not. R. Astron. Soc. **000**, 000–000 (0000) Printed 17 July 2000 (MN LATEX style file v1.4)

A strategy for finding gravitationally-lensed distant supernovae

Mark Sullivan,[1,2⋆] Richard Ellis,[2,1] Peter Nugent,[3] Ian Smail,[4] & Piero Madau[1]

[1] *Institute of Astronomy, Madingley Road, Cambridge CB3 OHA, UK*
[2] *California Institute of Technology, E. California Blvd, Pasadena CA 91125, USA*
[3] *E.O. Lawrence Berkeley National Laboratory, 1 Cyclotron Road, MS50-232, Berkeley, CA 94720, USA*
[4] *Department of Physics, University of Durham, South Road, Durham DH1 3LE, UK*

Accepted —. Received —; in original form —.

ABSTRACT

Distant Type Ia and II supernovae (SNe) can serve as valuable probes of the history of the cosmic expansion and star formation, and provide important information on their progenitor models. At present, however, there are few observational constraints on the abundance of SNe at high redshifts. A major science driver for the *Next Generation Space Telescope (NGST)* is the study of such very distant supernovae (SNe). In this paper we discuss strategies for finding and counting distant SNe by using repeat imaging of super-critical intermediate redshift clusters whose mass distributions are well-constrained via modelling of strongly-lensed features. For a variety of different models for the star formation history and supernova progenitors, we estimate the likelihood of detecting lensed SNe as a function of their redshift. In the case of a survey conducted with *HST*, we predict a high probability of seeing a supernova in a single return visit with either WFPC-2 or ACS, and a much higher probability of detecting examples with $z > 1$ in the lensed case. Most events would represent magnified SNe II at $z \simeq 1$, and a fraction will be more distant examples. We discuss various ways to classify such events using ground-based infrared photometry. We demonstrate an application of the method using the *HST* archival data and discuss the case of a possible event found in the rich cluster AC 114 ($z = 0.31$).

Key words: cosmology: observations – supernovae: general – gravitational lensing – galaxies: clusters: general

1 INTRODUCTION

Recent observational efforts to detect high-redshift (z) supernovae (SNe) have demonstrated their value as cosmological probes. The discovery and systematic study of faint, distant type Ia supernovae (SNe Ia) has led to renewed progress in constraining the cosmic expansion history (Garnavich et al. 1998; Perlmutter et al. 1999). The corrected Hubble diagram based on 42 SNe Ia from the Supernovae Cosmology Project (SCP, Perlmutter et al. 1999) yields a trend that strongly excludes the hitherto popular Einstein de Sitter universe and, for a spatially flat inflationary universe consistent with recent microwave background measurements (Hancock et al. 1998; de Bernardis et al. 2000), suggests a significant non-zero cosmological constant, $\Lambda \simeq 0.7$ (Perlmutter et al. 1999; Riess et al. 1998).

Such studies have now identified over 100 $z > 0.2$ SNe Ia, and, using controlled subsets of these SNe Ia samples, the first constraints are now emerging on the rate of their occurrence (Pain et al. 1996, 2000a). The observational determination of these rates is also important in many cosmological applications, for example as a diagnostic of the cosmic star formation history (SFH) and metal enrichment at high-z. SNe are independent of some of the biases associated with traditional tests based on flux-limited galaxy samples. Such biases are increasingly of concern given the steep luminosity functions now being witnessed for star-forming galaxies at all redshifts (Steidel et al. 1999; Sullivan et al. 2000) and, though there remain uncertainties in the correct treatment of dust in high-z type II supernovae (SNe II), they offer an alternative approach to studying the cosmic SFH.

SNe II are caused by the catastrophic core collapse of massive ($> 8\,M_\odot$) stars and, unlike SNe Ia, represent a direct probe of the massive SFH due to their short progenitor lifetimes – the evolution of the SNe II rate should closely match that of the cosmic SFH (Madau, Della Valle & Pana-

⋆ E-mail: ms@ast.cam.ac.uk

gia 1998; Sadat et al. 1998). Unfortunately, due to their intrinsically faint, heterogeneous nature, and their likely occurrence in dusty starburst regions, to date they have yet to be exploited in cosmological studies. However, as the predicted SNe II counts to faint survey limits (e.g. $I = 26$) will outnumber those of SNe Ia (Madau et al. 1998; Dahlen & Fransson 1999, Porciani & Madau 2000), the detection of SNe II at higher-z should become more practical as these fainter limits are attained – either through facilities such as the *NGST* (Dahlen & Fransson 1998) or via studies of the type introduced here.

SNe Ia, by contrast, arise from lower mass ($\simeq 3-8\,\mathrm{M}_{\odot}$) stars, and their rate depends strongly on the (as yet) unknown configuration of the progenitor system as well as the cosmic SFH. The SNe Ia rate therefore cannot yet be used to directly probe the SFH without a more detailed knowledge of the physics of SNe Ia explosions. The observed rate does however offer important implications for the possible progenitor models (Madau, Della Valle & Panagia 1998; Yungelson & Livio 1998) and, at $z > 1.5$, the predicted metal-dependency of the SNe Ia rate will provide valuable clues to the metal enrichment at high-z (Kobayahsi et al. 1998), as well as for the practicality of extending the Hubble diagram for more precise cosmological tests (Ruiz-Lapuente & Canal 1998).

The study of distant SNe of both types is one of the key programs underpinning the *NGST* (Dahlen & Fransson 1998). The optimum strategy for finding and studying SNe, particularly with respect to the investigation of SNe II and the SFH at $z > 1$, clearly depends on their abundance. In this paper, we suggest a strategy for producing the first observational constraints using existing facilities. The strategy proposed follows the idea proposed by Kolatt & Bartelmann (1998) and a similar approach used to locate faint sub-mm sources (Smail, Ivison & Blain 1997). By exploiting the magnification bias afforded by counting sources viewed through the cores of strong lensing clusters, fainter detection thresholds can be reached (Blain et al. 1999a). In the case of the sub-mm surveys the intrinsic flux limits achieved are fainter than those reached in more ambitious dedicated deep surveys. Adopting the same principle, optical searches for lensed SNe should provide a first glimpse of the evolution of SNe at high-z ahead of the launch of *NGST*.

A plan of the paper follows. In §2, we review the theoretical aspects of gravitational lensing as applicable to our proposed search and discuss the uncertainties associated with modelling SNe rates. This allows us to predict the source counts and redshift distribution for a survey with and without the effect of lensing. In §3 we discuss a possible application of the technique using the *HST* data archive. Only two rich clusters with the necessary lensing credentials have been multiply-visited in a single passband by *HST*, and we discuss one possible SNe found in each. In §4 we discuss the possibilities of classifying such detections via various follow-up strategies. We present our conclusions in §5. Throughout the paper, for consistency with the SCP results, we assume a lambda dominated cosmology of $\Omega_M = 0.3$, $\Omega_\Lambda = 0.7$, and $h = 0.5$, where $H_0 = 100\,h\,\mathrm{km\,s^{-1}\,Mpc^{-3}}$.

2 PREDICTED SUPERNOVA COUNTS

2.1 Introduction

The approach proposed is identical to that successfully employed in probing the faint sub-mm sources (Smail, Ivison & Blain 1997; Blain 1997). The core of a rich lensing cluster magnifies suitably-located background sources by factors of several. The critical difference with the sub-mm studies is that, for faint SNe studied at optical wavelengths, the exquisite angular resolution of *HST* is essential. The modest boost in detectability afforded by surveying through a massive foreground cluster significantly extends the mean detectable redshift. We primarily consider a search using the *HST* and the Wide Field Planetary Camera 2 (WFPC-2). The high spatial resolution, dark sky background and relatively large field-of-view ($5.71\,\mathrm{arcmin}^2$) of this telescope/instrument combination ensures faint survey limits can be reached in a reasonable exposure time. We also briefly consider the advantages of using the forthcoming Advanced Camera for Surveys (ACS) *HST* instrument, with a larger ($11.33\,\mathrm{arcmin}^2$) field-of-view.

In the rest of this section we investigate this observational approach by calculating the number density $N(m, z)$ of SNe of different types with and without the magnification produced by a massive cluster located at various redshifts. Below we introduce the theoretical aspects of both the lensing and the intrinsic SNe properties as a function of redshift.

2.2 Cluster Mass Models

The role of clusters in gravitational lensing has been reviewed by many authors (see, for example, Blandford & Narayan (1992) or Hattori, Kneib & Makino (1999) and references therein). A gravitational lens will distort and magnify a background source by an amount that depends on both the position of the source behind the cluster, and the relative redshifts of the source and the lens. This results in different background regions suffering different degrees of amplification, depending on their location behind the cluster. Through the location and spectroscopic identifications of multiply-imaged arcs (Mellier 1999), it is possible to correct for this effect by utilising a well-constrained cluster mass model to the accuracy required. These models involve multiple component mass distributions that are able to trace the potential well of a cluster and its more massive individual member galaxies (Kneib et al. 1996). The uncertainties in these best cases is currently $\simeq 10-20$ per cent (Blain et al. 1999a).

The degree of magnification that one can expect in the central regions of such massive clusters – the areas sampled when conducting lensed SNe searches – are typically of order $\mu \simeq 3$–4 for sources at $z_s = 2$ (Blain et al. 1999a), where μ is defined as the ratio of the magnified flux to the flux measured in the absence of lensing. However, this boost in sensitivity – or effective increase in the SNe number density as fainter SNe become brighter than the survey limiting magnitude due to amplification – is offset by the competing effect of depletion. This results in a decrease in the SNe number density, as the unit solid angle in the unlensed source plane *increases* by a factor of $1/\mu(z)$ in the lensed case, resulting in a *decrease* in the SNe number density by $1/\mu(z)$.

When attempting to determine a precise count rate of lensed sources, accurate modelling is essential. Here, we choose to model the cluster mass distribution more simply via a singular isothermal sphere (SIS), where the mass density ρ of the virialized dark matter halo of a cluster is given by $\rho(r) = \sigma_v^2/2\pi G r^2$, where r is a radial coordinate, and ρ is parameterized through σ_v, the one-dimensional velocity dispersion. The mass M of a halo interior to r is then $M(r) = 2\sigma_v^2 r/G$. This corresponds to a constant deflection angle for incident light rays, $\beta = 4\pi(\sigma_v/c)^2 = 28.8'' \, (\sigma_v/1000 \text{ km s}^{-1})^2$, always pointing towards the lens centre of symmetry. For a source that, in the absence of lensing, would be seen at an angular distance θ from this centre, the lens equation leads to an image at $\theta_+ = \theta + \theta_E$, with magnification $\mu_+ = \theta_E/\theta + 1$, where $\theta_E = \beta D_{ls}/D_{os}$ is the Einstein radius, and D_{os} and D_{ls} are the angular diameter distances between the observer, the lens, and the source. If the alignment is $\theta \leqslant \theta_E$ (strong lensing), a second image is produced at $\theta_- = \theta - \theta_E$ with magnification $\mu_- = \theta_E/\theta - 1$.

High-resolution N–body simulations have recently shown, however, that haloes formed through hierarchical clustering have a universal density profile which is shallower than isothermal (but still diverging like $\rho \propto r^{-1}$) near the halo centre, and steeper than isothermal (with $\rho \propto r^{-3}$) in its outer regions (Navarro, Frenk, & White 1997, hereafter NFW). This profile takes the form:

$$\rho(r) = \frac{\rho_c \, \delta_c}{(r/r_s)(1 + r/r_s)^2} \qquad (1)$$

where $\rho_c = 3\mathrm{H}^2(\mathrm{z})/8\pi\mathrm{G}$ is the critical density at the lens redshift, δ_c is a characteristic over-density, and $r_s = r_{200}/c$ is a scale radius, where c is a dimensionless number measuring the "concentration" of the halo, and the virial radius, r_{200}, is defined as the radius inside which the mass density is equal to $200\rho_c$. δ_c is related to c via

$$\delta_c = \frac{200}{3} \frac{c^3}{\ln(1+c) - \frac{c}{1+c}} \qquad (2)$$

We can then see that $M(r_{200}) = 800\pi\rho_c r_{200}^3/3$. The NFW haloes are thus defined by two parameters; c, and either r_{200} or M_{200}.

The lens equation for the NFW density distribution has been computed by several authors (Bartelmann 1996; Maoz et al. 1997; Wright & Brainerd 1999), and a good summary of its application can be found in Hattori et al. (1999). With respect to SIS profiles containing the same total mass and located at the same redshift, NFW lenses have smaller cross sections for producing multiple images, but this is compensated for by the fact that the average magnification of the images is higher for NFW haloes. In other words, NFW haloes are efficient magnifiers but poor image-splitters – a SIS profile underestimates the magnification obtained compared to an NFW profile.

In the following calculations, we model the lensing clusters using both SIS and NFW profiles. As a guide to the benefits of searching for SNe through clusters, we have explored two hypothetical cases: a survey conducted through a sample of (known) $\sigma_v = 1000 \, \mathrm{km\,s^{-1}}$ $z \simeq 0.2$ clusters, and a similar sample of $z \simeq 0.6$ clusters now being located through the MACS Survey (see for example Ebeling, Edge & Henry 2000). To meaningfully compare the magnifications of SIS and NFW profiles, we assume that for both profiles the clusters have identical masses interior to the virial radius, r_{200}. We then equate the expressions for $M(r)$ at r_{200} for both profiles, and hence set r_{200} for the NFW profile given a value for σ_v. For the NFW profiles, the concentration parameter c for each cluster is calculated for our cosmology using the FORTRAN routine *charden.f* provided by J. Navarro.

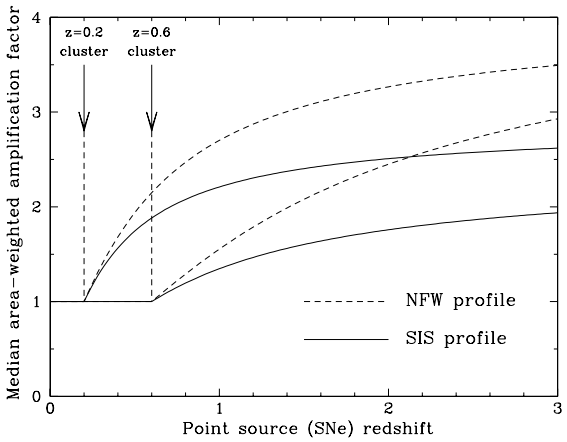

Figure 1. The median area-weighted magnification suffered by a point source as a function of redshift behind typical $\sigma_v = 1000 \, \mathrm{km\,s^{-1}}$, $z = 0.2$ and $z = 0.6$ clusters, for a search conducted using WFPC-2. The amplifications expected for both NFW and SIS profiles are shown.

The median area-weighted amplifications are calculated by considering a pixel matrix corresponding to the WFPC-2 CCD, and determining the amplification suffered by a background source were it to appear in each element. The median pixel amplification can then be found. Fig. 1 shows this amplification of a background source as a function of source redshift for two typical clusters. Typical median amplifications of $\mu \simeq 2$–3 are typical of $z \geqslant 1.5$ sources, corresponding to a brightening in magnitudes of $\simeq 1$.

2.3 Supernova Rates

We now estimate the number of SNe we would expect to find to a given survey magnitude limit at a given epoch, in the case of a blank field (i.e. without any significant lensing magnification) and through a rich cluster. We will not include those (unlensed) SNe that occur in the cluster galaxies, and will therefore underestimate the total number of new SNe that will be found in a lensed search. The number counts depend on both the intrinsic redshift-dependent SNe rate, and that period of the light curve during which time the SNe appears brighter than the survey search limit.

A number of workers have modelled the expected evolution in the SNe rate with redshift. Most have followed a similar route to that employed by Madau et al. (1998), who base their estimates on the observed luminosity densities which trace the cosmic star formation history (SFH). Using various diagnostics, the cosmic SFH can now be traced to high redshift ($z \simeq 4$), although some details remain controversial. As the progenitor lifetimes for SNe II are very short by cosmological standards, the SNe II rate can be calculated directly from the SFH provided an initial mass function (IMF) is

assumed. Here we adopt a Salpeter (1955) IMF with lower and upper mass cut-offs of $0.1\,M_\odot$ and $125\,M_\odot$ respectively.

In modelling the SNe II rate, the form of the cosmic SFH is critical. The original study of the evolution in the comoving star-formation rate based on optically selected galaxy surveys (Madau et al. 1996) suggested a sharp rise from $z = 0$ to a peak at $z \simeq 1$–2 by a factor of almost 10 (Lilly et al. 1996; Madau et al. 1996; Connolly et al. 1997), followed by a decline at high-z. However, more recent studies suggest that the evolution of the SFH up to $z \simeq 1.5$ may have been overestimated, perhaps only increasing by a factor of $\simeq 4$ (Tresse & Maddox 1998; Cowie, Songaila & Barger 1999; Sullivan et al. 2000), and that the SFR at high-z may be obscured due to large amounts of dust extinction (see, for example, Pettini et al. 1998 and Blain et al. 1999b). The form of this evolution to $z \simeq 2$ is crucial for our studies when predicting the SNe II rate.

We consider two illustrative SFHs. The first (SFH-I) is taken from Madau & Pozetti (2000), and provides a convenient analytical fit of the form:

$$\dot{\rho}_s(z) = \frac{0.23\, e^{3.4z}}{e^{3.8z} + 44.7}, \qquad (3)$$

which assumes an IMF lower mass cut-off of $\simeq 0.5\,M_\odot$ and an Einstein de Sitter (EdS) Universe. Multiplying by a factor of 1.67 will convert to a Salpeter IMF with a lower mass cut-off of $0.1\,M_\odot$. We convert the SFH to the Λ-dominated universe assumed here by computing the difference in luminosity density between an EdS Universe and our cosmology, and applying this correction to the fit above. The SFH fit matches most UV-continuum and Hα luminosity densities from $z = 0$ to $z = 4$, includes a mild correction for dust of $A_{1500} = 1.2$ mag ($A_{2800} = 0.55$ mag), and implies a local SNe II rate of $6.2 \times 10^{-5}\,\mathrm{SNe\,yr^{-1}\,Mpc^3}$, very close to that observed by Cappellaro, Evans & Turatto (1999).

However, the SFR evolution in this model to $z \simeq 1.5$ is both stronger, and results in a lower local SFR, than more recent measurements (Cowie et al. 1999; Sullivan et al. 2000). Accordingly, we also consider a second SFH (SFH-II) with a shallower evolution (a factor of $\simeq 4$ from $z = 0$ to $z \simeq 1.75$ in an EdS Universe, and constant thereafter), but one which over-produces the local SNe II rate. The SNe II rates as a function of redshift are shown in Fig. 2.

The SNe Ia rate is more difficult to model due to the uncertain nature of the progenitor system. The evolution expected depends critically on whether SNe Ia occur in double or single degenerate progenitor systems (for a review see Nomoto et al. (1999) and references therein), and there is much debate in the literature as to what form any evolution should take. We consider a commonly used empirical approach, and represent the uncertainty in terms of two parameters (Madau et al. 1998; Dahlen & Fransson 1999). The first is a delay time τ, between the binary system formation and SNe explosion epochs, which defines a (time-independent) explosion probability per white dwarf. The second is an explosion efficiency, η, which accounts for the fraction of binary systems that never result in a SNe. This efficiency η is constrained using a preliminary determination of the SNe Ia rate at $z = 0.55$ of $1.66 \pm 0.42\,h^3 10^{-4}\mathrm{Mpc^{-3}yr^{-1}}$ by Pain et al. (2000a) using a sample of 38 SNe Ia from the SCP (see also Pain et al. 2000b).

We consider two SNe Ia evolutions, shown in Fig. 2. The first has a small value of $\tau = 0.3$ Gyr (corresponding to a shallower decline at high-z,) whilst the second is a larger value of $\tau = 3.0$ Gyr, which produces a steeper drop-off. For comparison, the $z = 0.55$ rate of Pain et al. (2000a) is also shown in Fig. 2, together with the difference that arises from using the two SFHs, and how these histories tend to over or under-predict the local SNe rates.

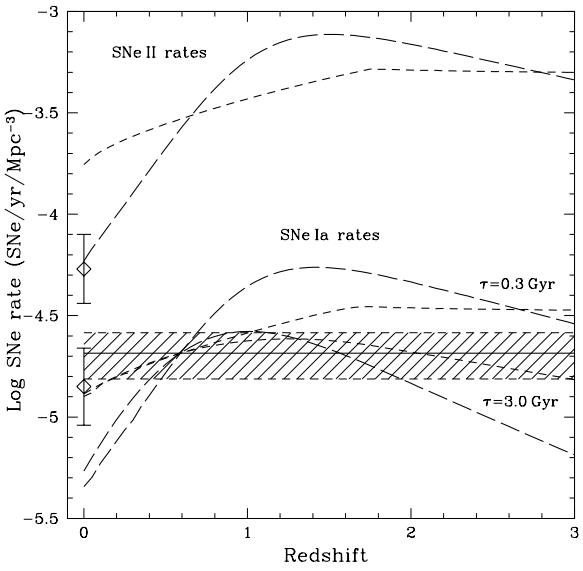

Figure 2. The adopted SNe rates as a function of redshift for both SNe II (top) and SNe Ia (bottom). The long dashed lines refer to rates derived using SFH-I, the short dashed lines refer to SFH-II. The SNe Ia rates are shown using two 'delay' times (τ = 0.3 & 3.0 Gyr). The horizontal solid line and shaded zone indicates the $z = 0.55$ SNe Ia rate and its uncertainty obtained by Pain et al. (2000a), used to calculate the efficiencies of the SNe Ia rates. Local SNe rates determined by Cappellaro et al. (1999) are shown for comparison.

While much published data exists for SNe Ia, by contrast there is a dearth of data for SNe II and a great variety in their spectra, peak magnitudes and light curves. For the purposes of this paper, we adopt the models of Gilliland, Nugent & Phillips (1999) (hereafter GNP) which incorporate recent light curve templates, k-corrections and luminosity functions for SNe Ia and II. These models include observed dispersions in the peak magnitudes of SNe Ia and II, which are included in our simulations of our SNe counts (see GNP for a full discussion of the models and simulations).

The major advantage to using GNP's models lies in the fact that the Spectral Energy Distributions (SEDs) are more realistic than those employed previously for rate calculations and follow the true temporal evolution of these objects. The SNe Ia template was constructed using data from *IUE* and *HST* (Cappellaro, Turatto & Fernley 1995; Kirshner et al. 1993) in the UV and a large number of ground-based observations in the optical. Spectrum synthesis calculations were carried out by PN for the SNe II's using the non-LTE code PHOENIX 9.0 (Hauschildt et al. 1997; Hauschildt, Baron, & Allard 1997). The spectra of SNe 1979C (Cappellaro, Turatto & Fernley 1995), 1992H and 1993W (courtesy D. Leonard) were fit at several epochs. The resultant fits of

these spectra provided a nice match to the observed data and yield a crude SED template for the SNe II's. The major emphasis of this effort was to model the UV as well as possible (this portion of the SED dominates in high-z searches using filters bluer than 1μm), since the simple assumption of blackbody SEDs has been shown to be quite inaccurate (see fig. 10 of GNP).

2.4 Results

We can now combine the two mass models from §2.2 and the various SNe rate models from §2.3 to estimate the number counts of SNe with and without the presence of a strong-lensing cluster.

As with blank-field surveys, searches such as those outlined here require two images of the same rich cluster, but with the two epochs of observation separated by a suitable amount to allow the SNe to become visible. When estimating the simple count rate of lensed high-z SNe, therefore, both forward (SNe in second image) and backward (SNe in first image) searches can be included, and to allow for the time dilation of the high-z SNe, we assume a time of at least 2 yrs between the two exposures. Table 1 gives the counts expected to survey limits of $I_{814} = 26.0$ & 27.0, assuming $z_{\rm cluster} = 0.2$ & 0.6.

When comparing lensed and unlensed counts, one of the key factors is the slope of the SNe number counts, $\alpha = {\rm d}\log{\rm N}/{\rm dm}$. For $\alpha > 0.4$, we expect lensing to increase the number counts, while for $\alpha < 0.4$, lensing will have the opposite effect (depletion). The slopes in our models depend on i) the intrinsic SNe properties, contained in the models of GNP, and ii) our assumed redshift evolution of the SNe number density. The models of GNP include the best-determined uncertainties in the SNe properties, for example in the dispersion of the peak SNe magnitude, and our simulations therefore account for this first uncertainty. The redshift evolution of the SNe numbers depends on which SFH we use, and, for SNe Ia, the value of the delay time, τ. By running simulations for the unlensed case, we find that typical values of α for SNe II for SFH-I are $\alpha \simeq 0.35$, and for SFH-II $\alpha \simeq 0.32$. There is little variation in these values between simulation runs.

The number-redshift relation is plotted in Fig. 3. As one would expect, the figure shows there is little difference in the rate of SNe up to $z_{\rm cluster}$. From $z_{\rm cluster}$ to $z \simeq 1$, the lensed counts are lower than those appropriate for blank field searches. This is due to the effect of depletion mentioned above, which unfortunately negates the lensing benefits. However, the important differences begin at $z > 1$, where we sample a fainter, more numerous population of SNe. Lensing has the principal effect of increasing the proportion of SNe found at high-z, bringing fainter, magnified examples into view. There is then a corresponding extension in the redshift distribution. For example, for the $z = 0.2$ NFW cluster, the mean redshift of detection changes from $z \simeq 0.70$ to $z \simeq 0.85$, and the number of detections at $z > 1$ increases from 20 to 31 per cent.

The numbers drop sharply by $z = 2$, even in the lensed case, due to the UV drop-off in the SNe spectrum being redshifted into the I_{814W} filter, which prevents the detection of higher-z SNe. We note that the use of *HST* and an infrared search would allow the detection of lensed $z > 2$ SNe which would be undetectable in the unlensed case.

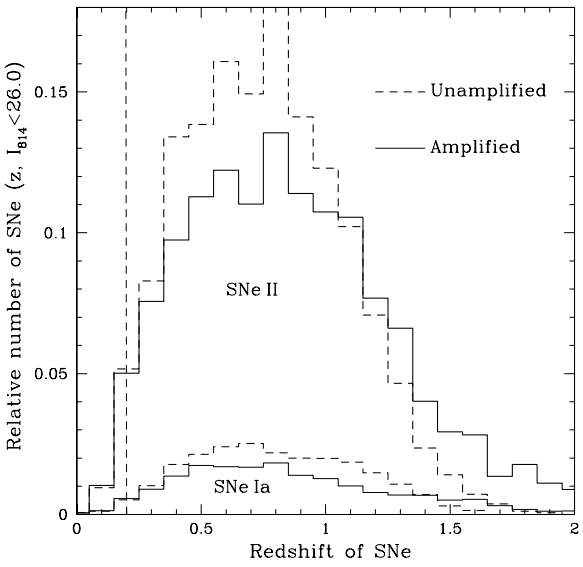

Figure 3. Redshift distribution of a search for lensed SNe generated from a Monte-Carlo simulation using the models of §2.2&2.3, to the limit $I_{814} = 26.0$. Both SNe II (heavy lines) and SNe Ia (light lines), magnified (solid line) and unmagnified (dashed line), are shown. The position of the (NFW profile) lensing cluster is shown by the dashed line at $z = 0.2$. Lensing alters the redshift distribution, resulting in the detection of a greater proportion of high-redshift SNe of both types. Only forward searches are included here.

3 APPLICATION TO THE *HST* ARCHIVE

Clearly, the number of detectable SNe depends on many variables which forms a strong motivation for this search, particularly in view of the need to quantify the high redshift rate in anticipation of detailed studies with *NGST*. A robust prediction from Table 1 is the high chance of discovering a new SNe during a repeat exposure of a previously studied lensing cluster. Specifically, to a reasonably modest magnitude limit (achievable in $\simeq$ 1–2 orbits), we can expect to discover 1 to 3 SNe per visit if we combine forward and backward searches.

To demonstrate the potential of such a search, we have analysed the *HST* data archive in the case of repeated observations of strong-lensing clusters for which mass models are available. Though there are few such repeated visits with the same filters, exposure times, enough images for a thorough cosmic-ray rejection and a satisfactory delay between the 'reference' and 'discovery' images, we have none the less discovered a candidate event in the rich cluster AC 114. The core of cluster AC 114 ($z = 0.31$) was observed on three occasions with WFPC-2 in the F702W filter (see Natarajan et al. 1998). The first two observations have total exposure times of 16.8 ks each and were taken on JD 50086.3 and 50089.3 (GO#5935). Both of these observations suffered from scheduling problems which resulted in the images having $\sim$ 4–5$\times$ the nominal sky background, limiting their sen-

Table 1. The predicted number of SNe to survey limits of $I_{814} = 26.0$ & 27.0 per WFPC-2 field for both a blank field and for a lensed survey (assuming $z_{\rm lens} = 0.2/0.6$ and the two lensing models). In each column the main entries refer to SFH-I and the values in parenthesis to SFH-II. The totals are the sum of IIL, IIP and a mean of the two Ia values. The bottom two lines show the expected counts for a survey using ACS and one of the scenarios. Also shown are the percentage of SNe found at $z > 1.0$ & $z > 1.5$. Both forward and backward searches are included.

Survey Limit	Lensing Model	*SNe Ia* $\tau = 0.3$	*SNe Ia* $\tau = 3.0$	*SNe II* (IIL+IIP)	Totals	Fraction (%) of SNe II with: $z > 1.0$	$z > 1.5$
$I = 26.0$, **WFPC-2**	Unlensed	0.32 (0.25)	0.22 (0.23)	1.44 (1.68)	**1.71 (1.92)**	23.2 (14.4)	1.4 (1.2)
	SIS, $z = 0.2$	0.25 (0.19)	0.18 (0.18)	1.30 (1.44)	**1.52 (1.63)**	30.3 (20.1)	4.0 (3.3)
	SIS, $z = 0.6$	0.31 (0.24)	0.22 (0.22)	1.47 (1.68)	**1.74 (1.91)**	26.4 (16.1)	2.6 (1.8)
	NFW, $z = 0.2$	0.23 (0.18)	0.16 (0.17)	1.25 (1.40)	**1.45 (1.58)**	31.0 (20.8)	4.6 (3.8)
	NFW, $z = 0.6$	0.30 (0.23)	0.21 (0.21)	1.46 (1.69)	**1.72 (1.91)**	26.9 (17.5)	3.2 (2.5)
$I = 27.0$, **WFPC-2**	Unlensed	0.56 (0.41)	0.38 (0.37)	2.86 (3.10)	**3.33 (3.49)**	32.7 (22.6)	3.8 (2.8)
	SIS, $z = 0.2$	0.42 (0.30)	0.27 (0.27)	2.34 (2.42)	**2.69 (2.71)**	37.7 (26.8)	6.4 (5.9)
	SIS, $z = 0.6$	0.51 (0.38)	0.36 (0.34)	2.85 (3.05)	**3.29 (3.41)**	34.5 (23.2)	5.4 (4.2)
	NFW, $z = 0.2$	0.38 (0.29)	0.25 (0.25)	2.20 (2.31)	**2.52 (2.58)**	37.9 (27.1)	7.1 (6.3)
	NFW, $z = 0.6$	0.49 (0.37)	0.33 (0.33)	2.77 (2.97)	**3.18 (3.34)**	33.5 (23.4)	5.4 (4.7)
$I = 26.0$, **ACS**	Unlensed	0.63 (0.50)	0.44 (0.46)	2.86 (3.33)	**3.39 (3.83)**	23.2 (14.4)	1.4 (1.2)
	SIS, $z = 0.2$	— (0.40)	— (—)	— (2.92)	— **(3.32)**	— (19.7)	— (3.0)

sitivity to $R_{702} \sim 26$ rather than the expected $R_{702} \sim 27$. As a result the cluster core was re-observed in Director's discretionary time (GO#7201) on JD 50747.5 for a further 15.6 ks.

Each of the observations comprises 6 single-orbit exposures in 3 pairs, each of which was spatially offset by 3 WFC pixels to enable the removal of hot pixels and similar artefacts. The observations are shifted so as to place the cluster cD on WFC4 (JD 50086.3), WFC2 (JD 50089.3) and on the boundary of WFC3–WFC4 (JD 50747.5) with space-craft orientations of PA(V3)=270, 270 and 220 degrees respectively. The three observations of the cluster core therefore sample very different areas of the WFPC-2 detectors, and the combination of this with the staggered timing makes this dataset well suited for searching for faint variable sources.

The data was reduced using the standard STScI pipeline, aligned with integer pixel shifts and then stacked using the STSDAS task CRREJ. The observations were calibrated using the F702W zero-point quoted by Holtzman et al. (1995). Finally, the three observations were rotated and aligned to allow a search for objects whose brightness varies between the visits.

The overlapping area between the three observations comprises a total area of roughly $80'' \times 80''$ and this region was searched for sources which were seen in both the JD 50086.3 and 50089.3 observations, but which were missing from the JD 50747.5 observation. The sequence is shown in Fig. 4. A variable point-source was identified – $4.6''$ (45 kpc) out in the halo of the central galaxy. The source brightness is $R_{702} = 26.4 \pm 0.15$ and 26.2 ± 0.15 in the earlier observations, but is fainter than $R_{702} > 27.6$ (3σ) in the observations taken 21 months later.

Though the object could be a SNe Ia in the envelope of the central cD galaxy, this would make it very faint unless caught at the end of its light curve. Note that the absence of a counterimage is not unexpected given the likely time delay involved.

Gal-Yam & Maoz (2000) have conducted a similar comparison of the strong-lensing cluster A 2218 which revealed another potential SNe. They detect a transient object ($V_{606W} = 22.8$) in an F606W March 1999 image, but which is absent from both an F606W January 2000 and an F702W September 1994 image. Though the relative brightness of this SNe suggests that it occurred in a $z = 0.1753$ cluster member galaxy, the usefulness of strategically surveying strong lensing clusters, for both lensed and unlensed SNe, is well demonstrated.

4 DISCUSSION

As we have seen in §2.4, there is a high degree of likelihood of detecting a new SNe in a repeat visit to a strong lensing cluster. We will now discuss possible follow-up strategies to any detections, and the type of science that can be achieved from these types of surveys.

As with early ground-based SNe Ia searches conducted in rich clusters (Hansen et al. 1989), it could be difficult to isolate the SNe, constrain its type, and determine a redshift. These early SNe searches were, however, essential in motivating astronomers to execute the later more ambitious programs, and before any concerted follow-up programs can be developed, it is first necessary to determine how many lensed SNe there may be and, where possible, their properties.

One of the primary benefits of the lensed search is the fact that faint, high-z SNe – which would otherwise be too faint for spectroscopic follow-up – are brightened sufficiently for spectroscopy to become feasible. We estimate that $\simeq 40$ per cent of $z > 1.5$ sources could be followed in this way, compared to $\simeq 5$ per cent without lensing. Such highly-lensed SNe such as these will typically be identifiable via their proximity to the cluster core. However, the magnitude of the faintest detected objects is still too faint for spectroscopic follow-ups on existing equipment. We need to examine various other methods of exploiting discoveries of lensed high-z SNe, and in particular, the possibilities of distinguishing the type of SNe in order to preferentially select either SNe Ia or II.

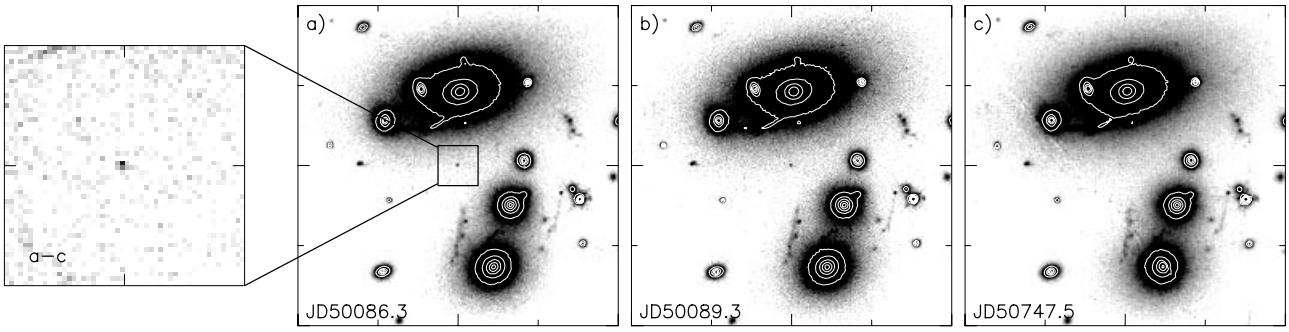

Figure 4. A demonstration of the technique applied to *HST* archival data on the lensing cluster AC 114 ($z = 0.31$). The detection $R_{702} = 26.3$ is found in both reference images on different parts of the detector (and hence cannot be an instrumental defect), but it is invisible ($R_{702} > 27.6$) in the image taken 21 months later.

New SNe will be caught at various stages on their light curve. We consider a statistical approach to classifying the detected SNe based on their colour distribution using a ground-based follow-up to any I_{814} detections using, as an example, the NIRC on the Keck-II telescope. Fig. 5 shows the $(I-K)$ – redshift distribution of detected SNe in the *HST* search using a simulation of many repeat visits to a $z = 0.2$ cluster, with the search criteria described in §2.4. The 'ridgeline' of blue SNe Ia colours arises from those nearer maximum light, with the SNe IIs redder than the Ia's. The ridgeline of redder SNe IIs arises from the fact that SNe IIs settle down to a constant colour after $\simeq 50$ days in the rest-frame. The other ridges and gaps in the diagram are a product of the light curve, for example there is a greater likelihood of detecting a SNe in a plateau phase than during a steep decline.

Fig. 6 indicates that the bulk of the reddest objects would be expected to be SNe with $z > 1$. These red objects would be detected in follow-ups using large ground-based telescopes in the K-band; i.e. those detected in K are likely to be higher-z and likely to be SNe II. Several photometric measurements can determine the rate of decline over a lunation and further constrain the type. The bluest detections will be SNe Ia observed close to maximum light. These may be further distinguished via the presence of a host galaxy whose redshift can be measured.

Although simply determining the number counts in searches such as these is important, it is interesting to consider other applications and their impact on our understanding of SNe.

The number counts of SNe Ia predicted is small, and it would be difficult to advance the existing Hubble diagram using this method. Accurate amplification corrections to the detected magnitudes would also be required. The mass models of most rich clusters are currently accurate to around 10–20 per cent, which would lead to uncertainties in the magnitudes of around 0.5 mag, insufficient for distinctions of a cosmological world model to be made. However, the *mere detection* of a high-z (and therefore red) SNe Ia would have important implications for the metallicity of the progenitor system. In a survey conducted to $I = 26.0\,(27.0)$ across 40 clusters, we would expect 5(8) SNe Ia to be found in the forward search, 2–3 of which would be at $z > 1$. Using these, the first tests of the high-z SNe Ia rate could begin.

A significant achievement would be the determination

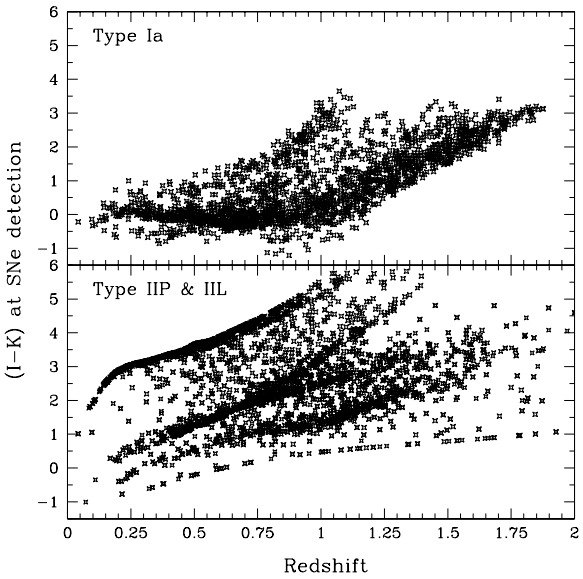

Figure 5. The simulated $I - K$ colour-redshift distribution for likely detections of SNe in a forward search behind a $z = 0.2$ rich cluster to $I_{814} \leqslant 26.0$. Each point represents a different detection, taking account of visibility, k-corrections, dust (SNe II only), and lens magnification effects. The lensing assumes the NFW profile discussed earlier. The distribution indicates the feasibility of ground-based follow-ups.

of the high-z SNe II rate, no measurement of which yet exists. The SNe Ia rate study of Pain et al. (2000a) at $z = 0.55$ shows that a sample of 38 SNe results in statistical and systematic uncertainties in the SNe rate of $\simeq 20$ per cent. Again, in a survey of 40 clusters, we would expect around 35(60) SNe II to be detected in the 'forward' search which could then be followed up from the ground. Of these $\simeq 10(17)$ would be SNe II at $z > 1$, and using the cluster mass models and an assumed cosmology, measures of the SFR at $z = 1$–2 could be made in an independent manner to existing measurements.

All these rates will be increased by using a larger field-of-view instrument, for example the 11.33 arcmin^2 Advanced Camera for Surveys (ACS). As an example, we repeated the simulations using this instrument and the $\tau = 0.3$ Gyr, SFH-II, $I = 26.0$ survey limit scenarios, shown as the bottom line

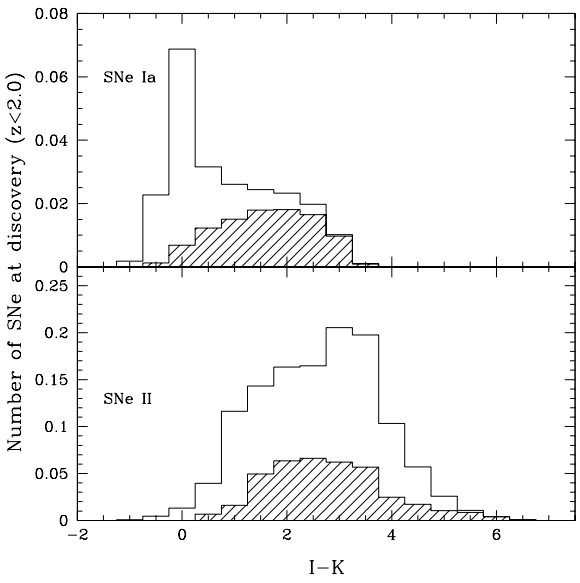

Figure 6. The distribution in $I-K$ of detected SNe for both Ia and II types. The shaded regions indicate the colours of the highest redshift objects ($z > 1$) and hence how follow-up strategies designed only to select high-z candidates might be imagined.

in Table 1. With this instrument, the predicted counts to $I = 26.0$ are as high as using the WFPC-2 to a survey limit of $I = 27.0$, and it becomes almost certain that a SNe will be found, and the larger field-of-view, and hence coverage of the lensing cluster, results in the potential discoverey of more high-z SNe.

5 CONCLUSIONS

In this paper, we have presented a technique for detecting SNe at $z > 1$ by utilising the magnification bias obtained by searching through rich clusters of galaxies. We summarise our main conclusions as follows:

(i) We have shown that a search utilising repeat *HST* WFPC-2 visits covering the cores of rich $z = 0.2$–0.6 clusters would reveal $\simeq$ 1–3 new SNe, of which $\simeq 80$ per cent will be of type II. Such a search will both increase the mean redshift of detected SNe, and will result in a threefold increase in the number of $z > 1.5$ SNe detected.

(ii) We have applied our technique using *HST* archival data, and have discovered a possible SNe event in the cluster AC 114 at $z = 0.31$.

(iii) We have discussed various follow-up strategies. The brightest events (to $I = 24$) can be followed spectroscopically using large ground-based telescopes, and a fraction of these will be highly lensed $z > 1.5$ SNe, which it would not be possible to follow-up without the lensing boost. For fainter SNe, K-band imaging will detect and select the redder, high-z SNe, and the light curve measurements can constrain the type.

(iv) We have discussed the potential scientific benefits of such a search, including the determination of the high-z SNe rates, constraints on the cosmic SFH, and the possibility of eliminating some SNe Ia progenitor models.

(v) We briefly consider the merits of using the Advanced Camera for Surveys, and find that even to $I = 26.0$, we expect $\simeq 3$ SNe per search (one of which will lie at $z > 1$) with a greater extension in the redshift range probed.

ACKNOWLEDGMENTS

We thank the anonymous referee whose comments improved this manuscript. We also thank Reynald Pain for providing his pre-publication value of the SNeIa rate, and Saul Perlmutter, Jean-Paul Kneib and Cristiano Porciani for their many helpful discussions in preparing this paper. This research used resources of the National Energy Research Scientific Computing Center, which is supported by the Office of Science of the U.S. Department of Energy under Contract No. DE-AC03-76SF00098.

REFERENCES

Bartelmann M., 1996, A&A, 313, 697
Blain A.W., 1997, MNRAS, 290, 553
Blain A.W., Kneib J-P., Ivison R.J., Smail I., 1999a, ApJ, 512, L87
Blain A.W., Smail I., Ivison R.J., Kneib J-P., 1999b, MNRAS, 302, 632
Blandford R.D., Narayan R., 1992, ARA&A, 30, 311
Cappellaro E., Turatto M., Fernley J., 1995, *IUE* – ULDA Access Guide No. 6: Supernovae, The Netherlands: ESA
Cappellaro E., Evans R., Turatto M., 1999, A&A, 351, 459
Connolly A.J., Szalay A.S., Dickinson M.E., Subbarao M.U., Brunner R.J., 1997, ApJ, 486, L11
Cowie L., Songaila A., Barger A.J., 1999, AJ, 118, 603
Dahlen T., Fransson C., 1998, in 'The *NGST*: Science Drivers and Technological Challenges', 34th Liège Astrophysics Colloquium, 98, 237.
Dahlen T., Fransson C., 1999, A&A, 350, 349
de Bernardis P., et al., 2000, Nature, 404, 955
Ebeling H., Edge A., Henry J.P., 2000, "Large scale structure in the X-ray universe" conf. proc., astro-ph/0001320
Gal-Yam A., Maoz D., 2000, IAU circular #7405
Garnavich P.M., et al., 1998, ApJ, 493, L53
Gilliland R.L., Nugent P.E., Phillips M.M., 1999, ApJ, 521, 30
Hancock S., Rocha G., Lasenby A.N., Gutierrez C.M., 1998, MNRAS, 294, 1
Hansen L., Jorgensen H.E., Norgaard-Nielsen H.U., Ellis R.S., Couch W.J., 1989, A&A, 211, 9
Hattori M., Kneib J-P., Makino N., 1999, Invited review in Progress of Theoretical Physics, in press, astro-ph/9905009
Hauschildt P.H., Baron E., Allard F., 1997, ApJ, 483, 390
Hauschildt P.H., Shore S.N., Schwarz G., Baron E., Starrfield S., Allard F., 1997, ApJ, 490, 803
Holtzman J.A., Burrows C.J., Casterno S.,Hester J.J., Trauger J.T., Watson A.M., Worthey G., 1995, PASP, 107, 1065
Ibata R.A., Richer H.B., Gilliland R.L., Scott D., 1999, ApJ, 524, L1
Kirshner R., et al., 1993, ApJ, 415, 589
Kneib J-P., Ellis R.S., Smail I., Couch W.J., Sharples R.M., 1996, ApJ, 471, 643
Kolatt T., Bartelmann M., 1998, MNRAS, 296, 763
Kobayashi C., Tsujimoto T., Nomoto K., Hachisu I., Kato M., 1998, ApJ, 503, L155
Lilly S.J., Le Fèvre O., Hammer F. Crampton D., 1996, ApJ, 460, L1
Mellier Y., 1999, ARA&A, 37, 127

Madau P., Pozzetti L., 2000, MNRAS, 312, L9
Madau P., Ferguson H.C., Dickinson M.E., Giavalisco M., Steidel C.C., Fruchter A., 1996, MNRAS, 283, 1388
Madau P., della Valle M., Panagia N., 1998, MNRAS, 297, 17
Maoz D., Rix H-W., Gal-Yam A., Gould A., 1997, ApJ, 486, 75
Natarajan P., Kneib J-P., Smail I., Ellis R.E., 1998, ApJ, 499, 600
Navarro J.F., Frenk C.S., White S.D.M., 1997, ApJ, 490, 493
Nomoto K., Umeda H., Hachisu I., Kato M., Kobayashi C., Tsujimoto T., 1999, in Truran J., Niemeyer J.,eds, 'Type Ia Supernovae: Theory and Cosmology', Cambridge University Press, astro-ph/9907386
Pain R., et al., 1996, ApJ, 473, 356
Pain R., et al., 2000a, in preparation
Pain R., et al., 2000b, Moriond Conf. Proc. Janurary 2000, in press
Perlmutter S., et al., 1999, ApJ, 517, 565
Pettini M., Kellogg M., Steidel C., Dickinson M., Adelberger K., Giavalisco M., 1998, ApJ, 508, 539
Porciani C., Madau P., 2000, ApJ, 532, 679
Riess A.G., et al., 1998, ApJ, 504, 935
Ruiz-Lapuente P., Canal R., 1998, ApJ, 497, L57
Sadat R., Blanchard A., Guiderdoni B., Silk J., 1998, A&A, 331, L69
Salpeter E.E., 1955, ApJ, 121, 161
Smail I., Ivison R.J., Blain A.W., 1997, ApJ, 490, 5
Steidel C., Adelberger K., Giavalisco M., Dickinson M., Pettini M., 1999, ApJ 519, 1
Sullivan M., Treyer M., Ellis R.S., Bridges T., Donas J., Milliard B., 2000, MNRAS, 312, 442.
Tresse L., Maddox S.J., 1998, ApJ, 495, 691
Wright C.O., Brainerd T.G., 1999, ApJ submitted
Yungelson L.R., Livio M., 1998, ApJ, 497, 168